Auditory Cortex Controls Sound-driven Innate Defense Behavior through Corticofugal Projections to Inferior Colliculus

Xiaorui R. Xiong[1,2,*], **Feixue Liang**[1,5,*], **Brian Zingg**[1,2,*], **Xu-ying Ji**[1,5], **Leena A. Ibrahim**[1,2], **Huizhong W. Tao**[1,4,#], and **Li I. Zhang**[1,3,#]

[1]Zilkha Neurogenetic Institute, Keck School of Medicine, University of Southern California, Los Angeles, 90033, USA

[2]Neuroscience Graduate Program, Keck School of Medicine, University of Southern California, Los Angeles, 90033, USA

[3]Department of Physiology and Biophysics, Keck School of Medicine, University of Southern California, Los Angeles, 90033, USA

[4]Department of Cell and Neurobiology, Keck School of Medicine, University of Southern California, Los Angeles, 90033, USA

[5]Department of Physiology, School of Basic Medical Sciences, Southern Medical University, Guangzhou 510515, China

Abstract

Defense against environmental threats is essential for animal survival. However, the neural circuits responsible for transforming unconditioned sensory stimuli and generating defensive behaviors remain largely unclear. Here, we show that corticofugal neurons in the auditory cortex (ACx) targeting the inferior colliculus (IC) mediate an innate, sound-induced flight behavior. Optogenetic activation of these neurons, or their projections in the IC, is sufficient for initiating flight responses, while inhibition of these projections reduces sound-induced flight responses. Corticocollicular axons monosynaptically innervate neurons in the cortex of the IC (ICx), and optogenetic activation of projections from the ICx to the dorsal periaqueductal gray is sufficient for provoking flight behaviors. Our results suggest that ACx can both amplify innate acoustic-motor responses and directly drive flight behaviors in the absence of sound input through corticocollicular projections to ICx. Such corticofugal control may be a general feature of innate defense circuits across sensory modalities.

[#]Correspondence should be addressed to: L.I.Zhang (liizhang@usc.edu) or H.W.Tao (htao@usc.edu).
[*]These authors contributed equally to this study.

Introduction

Defense against harm is a fundamental requirement to survival. Natural threatening stimuli such as odors of predators[1–3], looming shadows[4], or warning sounds emitted by co-species[5,6], can automatically invoke species-wide defensive behaviors including freezing, fleeing and fighting[7,8]. These innate behaviors are controlled by hard-wired, genetically preprogrammed innate defense circuits that have evolved through natural selection. Biologically insignificant or neutral sensory stimuli (i.e. conditioned stimuli, CS) can acquire the ability to elicit defensive behaviors through the process of Pavlovian conditioning, when they occur in conjunction with biologically significant threats (i.e. unconditioned stimuli, US).

Neural circuits for unconditioned and conditioned behaviors likely share common components, e.g. the centers for organizing defensive behavioral responses such as the periaqueductal gray (PAG)[2,9] and the motor pathways for producing behavioral reactions. Previous studies have largely focused on the neural mechanisms for learned defensive behaviors such as fear conditioning. For fear conditioning, it is generally believed that the sensory inputs from CS such as a tone or flash of light are processed in the cortex[10] and are then transmitted to the amygdaloid complex, where the association between CS and US occurs[11]. Outputs from the central nucleus of the amygdala then project to the ventrolateral PAG (PAGvl) to produce fear behaviors[12–16]. It is surprising to note that, for many innate defense behaviors, the neural circuits responsible for producing defensive behaviors in response to the US, particularly for non-olfactory modalities, are considerably less well-understood[1,11].

In this study, we address a general question about innate defensive behaviors: whether the sensory cortex contributes to the generation of these behaviors, and if so what are the underlying neural pathways. By focusing on a sound induced innate flight behavior and exploiting modern optogenetic tools with high spatial and neuronal specificity, we explored the role of auditory cortex (ACx) in the generation of the innate defensive behavior and dissected the underlying neural pathway. Our results reveal that ACx can drive the innate defensive behavior via the corticofugal projections to the cortex of IC, which then connects to the PAG to initiate the flight response. Our study elucidates a previously unrecognized role of corticofugal projections in mediating innate sensory-motor responses, which may be general across sensory modalities.

Results

A sound induced innate defensive behavior

By examining acoustically induced behavioral reactions, we observed that a moderately loud sound could reliably invoke flight responses in naïve mice. As shown in Fig. 1a–d, during free exploration in a chamber, a broadband noise [1–64 kHz; 80 dB sound pressure level (SPL), 5-s duration] delivered from a hidden speaker in the chamber resulted in a flight behavior away from the sound to another connected chamber. The animal typically remained on the far side of the second chamber for the remainder of the noise. No obvious freezing behavior was observed prior to the flight, or during the noise presentation. Such innate

defensive behavior (i.e., fleeing from potential threats) was observed in all of the mice tested (n = 7).

To study the neural circuits for this sound-induced flight behavior, we developed a head-fixed preparation[17–19] so that the behavioral response could be easily quantified. Head-fixed mice were habituated to rest or run on a flat turntable, and the running speed was recorded in real time (Fig. 1e). A 5-s noise presented at 50 dB SPL on one side of the animal (with the contralateral ear plugged) induced running approximately 1s after the onset of noise, as shown by the increase in turntable speed (Fig. 1f, black). Noise presented at a higher intensity (80 dB SPL) resulted in faster running speeds and a more rapid response initiation (Fig. 1f, magenta). The sound-induced running behavior was further confirmed by examining recorded video images. By varying the intensity of noise in a randomized order, we determined the relationship between peak sound-induced running speed and stimulus intensity (Fig. 1g), which could be modeled using a hyperbolic ratio function (see Methods). We defined the intensity at which the speed reached the half-maximum value as I_{50} (Fig. 1g). We also measured T_{50}, defined as the time when the sound-induced running speed reached the half-maximum value, relative to the onset of noise (Fig. 1f). T_{50} decreased with increases of stimulus intensity (Fig. 1h), indicating that increasing noise intensity resulted in faster initiation of the flight response. Such noise-induced flight behavior was reliably observed in a total of 35 head-fixed mice, although there was substantial variability in the induced running speed (V), T_{50}, and I_{50} across mice (Fig. 1i–k respectively). There was no correlation between sound-induced speed and the baseline speed (correlation coefficient = 0.19, Fig. 1l), indicating that the sound-induced running was relatively independent of the initial status of the animal. When both ears were left open, noise at 80 dB SPL produced similar running speeds as in the condition of unilateral plugging (Supplementary Fig. 1a). The behavioral response under our experimental condition (with an inter-stimulus interval of 30 sec) was relatively stable over 100 min duration, without obvious adaptation, but reduced responses were observed over time when a shorter inter-stimulus interval was applied (Supplementary Fig. 1b). Further, a 5 kHz pure tone stimulus presented at 80 dB SPL evoked similar flight responses as noise (Supplementary Fig. 1c–d), suggesting that flight responses may be generally induced by loud sounds when there are escape routes.

IC mediates the sound-triggered flight response

Previous studies have implied that the IC may be involved in acoustically induced defensive behaviors, since electric or chemical stimulation of the IC can result in defense-like responses[7]. We therefore examined the involvement of the IC in the sound-induced flight behavior by silencing the IC with local microinjections of muscimol (see Methods). Using fluorescent muscimol, we confirmed that muscimol was largely restricted to the IC structure after the injection (Fig. 1m). The effectiveness of silencing was confirmed by loose-patch recordings from neurons across different depths of the IC (Fig. 1n). Silencing the IC contralateral to the stimulated ear largely reduced noise-induced running (Fig. 1o–p). The small residual response (Fig. 1p) might be attributed to the incomplete silencing of IC, e.g. the auditory pathways through the other (ipsilateral) IC were intact. Indeed, when we silenced the IC bilaterally, the running response was almost completely abolished (Fig. 1q).

These data suggest that the sound-induced flight behavior is initiated at or above the level of the IC.

ACx amplifies and directly drives defensive flight behavior

For any sound-induced behavior, a straightforward question to ask is whether the ACx is involved. The ACx processes ascending acoustic information relayed from the IC[20], and may contribute to the evaluation of threat signals. To silence the ACx, we locally injected muscimol, which diffused mainly throughout the primary auditory cortical region (A1), leaving subcortical structures and other cortical areas (e.g. motor cortex) unaffected (Fig. 2a). Loose-patch recordings confirmed that sound-evoked spike responses in the A1 were effectively eliminated (Fig. 2b). On the other hand, the responses in the auditory thalamus (the ventral part of the medial geniculate nucleus (MGBv)) remained intact (Fig. 2c), indicating that the ascending auditory pathway from the IC to MGBv and then to ACx was not affected by cortical muscimol injections. Silencing the ACx contralateral to the sound source markedly attenuated, but did not abolish, the sound-induced flight response (Fig. 2d), resulting in a rightward shift of the speed-intensity curve and a reduction of the maximum induced speed (Fig. 2e). On average, V was reduced by 47% after silencing the ACx (Fig. 2f). Moreover, both T_{50} and I_{50} increased (Fig. 2g,h). Silencing the ACx bilaterally resulted in a similar reduction in V (data not shown). In control experiments where saline was injected into the ACx, or muscimol into the visual cortex, no significant change in the behavioral response was observed (Supplementary Fig. 2).

We also applied another method of cortical silencing, by optogenetically activating parvalbumin (PV) positive inhibitory neurons[21,22]. We injected an adeno-associated viral vector encoding double-floxed inverted channelrhodopsin 2 (ChR2)[23] fused with EYFP (AAV-DIO-ChR2-EYFP) into the ACx of PV-Cre mice (Fig. 2i). PV neurons were optically activated by blue LED light (470 nm) applied to the cortical surface through an optic fiber. Loose-patch recordings of excitatory cells in deep layers of A1 (see Methods) confirmed that their responses could be silenced by a train of pulses of blue LED illumination (10 ms pulse duration, 10 Hz) (Fig. 2j). We interleaved noise stimulation with and without blue LED illumination, and found that LED illumination markedly reduced noise-induced running speeds (Fig. 2k). On average, the peak induced running speed was reduced by 40% (Fig. 2l), comparable to the effect of muscimol silencing (Fig. 2f). Together, these results suggest that subcortical structures are partially responsible for producing the behavioral response, and that ACx-mediated processes amplify and accelerate the response. Additionally, these results raise the interesting possibility that ACx can directly drive the defensive behavior.

Since layer 6 of the primary sensory cortex has been shown to play a primary role in controlling the gain of thalamocortical inputs[17] and layer 2/3 in sending information to higher cortical areas for sensory processing[24], we suspected that layer 5 (L5), another cortical output layer, might play a prominent role in mediating the observed behavior[25]. To test this hypothesis, we injected the AAV-DIO-ChR2-EYFP into the A1 region of a L5-specific Cre driver mouse line, Rpb4-Cre[26], in order to optically activate only this output layer (Fig. 2m). The EYFP-labeled L5 neurons exhibited a long apical dendrite ascending

towards layer 1 (Fig. 2m), consistent with previous morphological studies of L5 pyramidal cells[27,28]. We applied blue LED light to the cortical surface, with the tip of the optic fiber covered by dark stained agar to minimize the leakage of LED light (see Methods). LED illumination induced spiking responses of L5 neurons (Fig. 2n and Supplementary Fig. 3a–b). Surprisingly, the optical activation of L5 neurons induced running (Fig. 2o–p). This behavioral response depended on the LED light intensity, and was not evoked at low LED powers (Supplementary Fig. 3c–d). In addition, the running behavior could not be attributed to visual effects, as control mice injected with AAV-GFP did not respond to the same LED illumination (Supplementary Fig. 3e–f). In view of the above results, we reasoned that a common neural pathway through the same subcortical sensory structures might enable the ACx to amplify the sound-induced flight behavior and to drive behavioral output in the absence of sensory input.

Involvement of corticofugal projections to the cortex of IC

Since ACx connects to the IC through corticofugal projections originating from L5[29,30], we directly examined whether L5 neurons can drive the flight behavior via the corticocollicular projections. In the Rbp4-Cre mice injected with AAV-DIO-ChR2 in the A1 region, we found that the EYFP-expressing corticocollicular axons in the IC were mainly distributed in the IC cortex, the shell region surrounding the central nucleus (i.e. ICC) (Fig. 3a). To test whether the corticocollicular axons innervate IC neurons, we performed whole-cell voltage-clamp recordings in slice preparations, and stimulated corticocollicular axon terminals by illuminating blue LED light onto the entire IC region (see Methods). The slices were bathed in 1 μM TTX and 1 mM 4-AP so that polysynaptic responses were blocked[31]. We found that a 10-ms pulse of LED light induced robust excitatory postsynaptic currents (EPSCs) in neurons in the IC cortex (Fig. 3b), demonstrating that corticocollicular axons indeed monosynaptically innervate these cells. On the other hand, no EPSCs were observed in ICC neurons recorded in the same slices, indicating that the probability of ICC neurons being innervated by corticocollicular axons is much lower compared with IC cortex neurons, consistent with the sparseness of corticocollicular axons in the ICC region (Fig. 3a).

We next examined whether local activation of corticocollicular axon terminals in the IC could directly drive the flight behavior. In head-fixed Rbp4-Cre animals injected with AAV-DIO-ChR2, we applied a train of LED light pulses (10 ms duration, 10 Hz) onto the IC surface for 5 sec, while the ACx on the same side had been silenced with muscimol to prevent potential antidromic stimulation of L5 neurons (Fig. 3c). Under this condition, the LED illumination increased spiking activity of neurons in the IC cortex, but not in the ICC (Fig. 3d). Optogenetic activation of corticocollicular axon terminals in the IC evoked running (Fig. 3e), with similar running speeds as those induced by noise (Fig. 3f), but with longer latencies (Fig. 3g, T_{50}, 2.62 ± 0.56 s vs 1.44 ± 0.45 s, $P < 0.01$, t test). The latter could be due to a longer time needed for activating a sufficient number of neurons in the IC cortex under our current optical stimulation conditions as compared to natural sound stimulation. Together, our data suggest that activation of corticocollicular projections is sufficient for driving the flight behavior.

To further confirm that corticocollicular projections are involved in the sound-induced flight behavior, we injected AAV-flexed-ArchT-GFP[32] into the ACx of Rpb4-Cre mice to suppress spiking activity of L5 neurons (Fig. 3h). In cortical slices, green LED light illumination (530 nm, 1 s) caused a large hyperpolarization of the membrane potential in fluorescence-labeled L5 pyramidal neurons (-33 ± 8 mV, n = 10 cells), confirming the effectiveness of ArchT expression. In head-fixed animals, green LED light illumination onto the auditory cortical surface reduced the sound-induced running speed by 40% (Supplementary Fig. 4a–d). Consistently, illumination on the IC surface suppressed sound-evoked spike responses of IC cortex neurons (Fig. 3h–i), and reduced the sound-induced behavioral response by 27% (Fig. 3j–l). Possibly due to less efficient inhibition at axon terminals, the level of reduction was smaller compared to the illumination on the cortical surface. The effects of activation and suppression of the corticocollicular projections to the IC with various methods (Supplementary Fig. 5) together strongly indicate their involvement in the sound-induced flight behavior.

IC cortex drives the flight behavior

The IC structure is anatomically separated into the ICC and the shell region (IC cortex). The latter has been implicated in multisensory interactions[29,33]. We have now shown that activation of corticocollicular axons can drive flight behavior, and that IC cortex neurons are directly innervated by corticocollicular axons (Fig. 3a–b). To confirm that the IC cortex is a sensory hub mediating the sound-induced behavior, we injected an AAV encoding nonfloxed ChR2 driven by a CaMKII promoter into the dorsal cortex of the IC (Fig. 4a). ICC neurons were largely uninfected (Fig. 4a, right panel). Whole-cell recordings in IC slices indicated that blue LED light (10 ms, 10 Hz) could reliably induce spiking of infected IC cortex neurons (n = 10 cells) (Fig. 4a, right bottom), while no excitatory currents were observed in ICC neurons (n = 10 cells, data not shown). These results demonstrate the specificity of ChR2 expression in the IC cortex.

In head-fixed animals, optogenetic activation of IC cortex neurons (and ACx silenced with muscimol) induced running (Fig. 4b–d). In a second set of experiments, we suppressed spiking activity of IC cortex neurons by injecting AAV–CAG-ArchT-GFP into the IC cortex (Fig. 4e). Green LED light illumination of ArchT-expressing neurons resulted in a large membrane hyperpolarization of 35 ± 9 mV in these neurons (n = 10 cells) (Fig. 4e, right bottom). In head-fixed animals, green LED illumination (5s duration, 10 Hz) of the IC surface largely reduced the sound-evoked flight response (Fig. 4f). On average, there was a 37% reduction in the peak induced running speed (Fig. 4g), with the latency of the behavioral response prolonged (Fig. 4h). It should be noted that it is usually difficult to achieve complete inactivation with ArchT expression. Nonetheless, the above data further suggest that the IC cortex is required for the sound-induced flight behavior.

We also examined how ICC might contribute to the flight behavior. We injected the AAV encoding nonfloxed ChR2 into the ICC (Fig. 4i). Recordings from infected ICC neurons in slice preparations confirmed that they could be activated by blue LED light (n = 8 cells) (Fig. 4i, right bottom). Notably, LED illumination of the IC and thus activation of ICC neurons evoked a running response similar to that induced by noise except for a longer

response delay (Fig. 4j–l). However, after muscimol was injected into the ACx, this response disappeared (Fig. 4j–k). Since the MGBv relays ascending auditory input from the ICC to the ACx, we further examined the effect of silencing the MGB with muscimol on the response induced by the optical activation of the ICC. The behavioral response was largely reduced (Supplemental Fig. 6), similar to the effect of silencing the ACx. Together, these results suggest that ICC by itself does not directly mediate the flight behavior. It mainly relays ascending auditory input into the ACx via the MGB, and the ACx in turn activates the IC cortex via the corticocollicular projections to modulate the running behavior.

IC cortex drives the midbrain defense system

What are the downstream targets of the IC cortex that produce the flight behavior? IC cortex neurons primarily project their axons to the MGB[29], intermediate and deep layers of the superior colliculus (SC), and the dorsal-lateral part of the PAG (PAGd) ventral to the SC (Fig. 5a). The PAG region ventral to the IC was not innervated by the projections from the IC cortex[29]. Previously the SC and PAG have been implicated in the midbrain defense system, as electrically or chemically stimulating these nuclei could produce a variety of defense-like behaviors[7]. It is therefore possible that IC cortex drives the flight behavior by activating the SC and PAGd. Supporting this notion, in midbrain slices from mice injected with AAV-ChR2 in the IC cortex, blue LED illumination elicited large monosynaptic EPSCs in PAGd neurons, with their amplitudes consistently reaching hundreds of picoamperes or above (Fig. 5b). Neurons in the intermediate and deep layers of SC also received direct excitatory input from the IC cortex, although the input was much weaker compared to that to the PAGd (Fig. 5b). In addition, *in vivo* recording of local field currents (LFCs) in the PAGd and deep layers of SC indicated that these nuclei received sound-driven synaptic inputs (Fig. 5c). The input to the PAGd was much stronger than that to the SC (Fig. 5c), consistent with the *ex vivo* result (Fig. 5b). In addition, the amplitude of high-intensity noise evoked LFC in the PAGd was found to be significantly reduced after ACx was silenced by muscimol (Fig. 5d), indicating that ACx amplified the sound-evoked responses in the PAGd. This is consistent with the result that ACx activity amplified the sound-evoked flight behavior (Fig. 2f, 2l).

To address whether ACx and IC cortex mediate the flight behavior via the PAGd and SC, we first examined their responses to activation of corticocollicular axons. In Rbp4-Cre mice injected with AAV-DIO-ChR2 in the ACx, we applied blue LED illumination onto the IC surface, with the ACx silenced with muscimol (Fig. 5e). The optogenetic activation of corticocollicular axon terminals in the IC produced LFC responses in the IC cortex, PAGd and deep layers of SC (Fig. 5f), confirming the L5→IC cortex→PAGd/SC pathway. Again, the evoked LFC responses were stronger in the PAGd than in the SC (Fig. 5g). In another set of experiments, we injected AAV-ChR2 into the IC cortex. We then implanted an optic fiber in the midbrain rostral to the IC to illuminate the PAGd area ventral to the SC, thus to specifically activate axon terminals from the IC cortex in this region (Fig. 5h). Muscimol was injected to silence the IC cortex region expressing ChR2 (Fig. 5h). Notably, LED illumination alone evoked running (Fig. 5i–j), and the T_{50} of the average response trace appeared similar as that under the optogenetic activation of corticocollicullar axons in the IC and of IC cortex neurons (Fig. 5k). Although it would be difficult to separately illuminate

the SC without affecting the PAGd (see Fig. 5a), it is likely that the IC cortex to SC projection can also contribute to the flight behavior, as anatomical studies have indicated that deep layers of SC project to the PAGd[34,35]. Together, our data suggest that IC cortex directly drives the midbrain defense system, in particular the PAGd, to produce the sound-triggered flight behavior.

Corticofugal projections to the SC are unlikely involved

Anatomical evidence suggests direct corticofugal projections from the ACx to the SC[29,30]. As electric or chemical stimulation of the SC also results in some types of defense-like behavior[7], we further examined possible involvements of corticofugal projections to the SC in the observed behavior. In Rbp4-Cre mice with AAV-DIO-ChR2 injected in the ACx, we only observed weak fluorescence in the intermediate and deep layers of SC (Fig. 6a), suggesting that only a small population of auditory cortical neurons project to the SC. Double retrograde labeling (see Methods, Fig. 6b) revealed that there was limited overlap between L5 corticofugal neurons projecting to the IC and those to the SC (Fig. 6c). Overall, only about 2% of IC-projecting cortical neurons also projected to the SC. Moreover, about 66% of IC-projecting neurons were also Cre positive, and a small fraction (about 10%) of IC-projecting neurons came from layer 6 (Fig. 6c). The number of labeled IC-projecting neurons was estimated to be about twenty times that of SC-projecting neurons. IC-projecting neurons were found to be more enriched in L5 of primary as opposed secondary auditory areas (Supplementary Fig. 7), consistent with previous anatomical studies[36] and recent neural tracing results, e.g. in the Allen database (connectivity.brain-map.org) and the mouse connectome project (www.mouseconnectome.org). Local activation of corticofugal axons in the SC failed to invoke running (Fig. 6d–f), which could be explained by the relatively sparse ACx-SC projection. Together, the corticofugal projection to the SC unlikely contributes directly to the sound-triggered flight response. It is possible that corticofugal projections to different subcortical targets play distinct roles in various brain functions[25].

Discussion

Flight behaviors invoked by threatening sensory stimuli have been observed in various species[8]. However, the sensory cortical control of innate defense behaviors induced by unconditioned sensory inputs and the underlying neural pathways remains unclear. In this study, we demonstrated that ACx can drive the IC cortex via corticofugal projections, and that the IC cortex connects to the midbrain defense system to generate innate sound-induced flight behaviors. Our results elucidate an innate defense circuit that links the auditory sensory system and motor outputs, by which the auditory cortex mediates sound-induced defense behaviors (Fig. 7).

The defense circuit identified in this study could be distinguished from that for other types of acoustically induced defensive responses, such as the acoustic startle response (ASR) and freezing. ASR is triggered by extremely loud sounds (> 80dB SPL), has a fast onset (with a delay that can be as short as 10 ms) and is only transient (lasting approximately 100ms)[37,38]. ASR is mediated by brainstem auditory nuclei below the level of the IC, e.g. dorsal and ventral cochlear nucleus as well as the caudal pontine reticular nucleus[37,38]. The most-

studied freezing responses are those generated after fear conditioning, in which acoustic stimuli are paired with foot shocks[13]. It is interesting to note that in our study, sound stimuli only induced flight responses; we never observed freezing behavior in response to our sound stimuli. This observation is in fact consistent with the known function of some components of the identified neural pathway, in particular the IC cortex to PAGd connection. Previous studies have suggested that the dorsal part of the PAG is involved in organizing flight responses, while freezing responses are primarily mediated by the ventral part of the PAG (PAGv)[34,35], which is not a direct target of the IC cortex. It is therefore likely that the sound-induced freezing behavior after fear conditioning involves a different neural circuit, which recruits the PAGv.

In this study, we show that activation of corticofugal projections to the IC can directly initiate a flight response, and that silencing the ACx reduces the sound-induced flight response by nearly half. One parsimonious explanation is that the ACx amplifies the sound-induced flight response via the same neural pathway as it drives the behavior. The fact that the IC cortex itself receives ascending auditory information (in particular, from nuclei of the lateral lemniscus)[39] can explain the result that silencing the ACx does not completely eliminate the sound-induced flight response. Our results suggest that via the corticofugal projections, the ACx may provide evaluative information about the threatening nature of acoustic signals to the IC cortex, reinforcing the responses in the midbrain. Given that the earliest sound-evoked spike responses occur in L5 among cortical layers[28], this may allow the ACx to rapidly transform threatening signals to behavioral commands.

In the central auditory system, massive corticofugal feedback projections run in parallel with the ascending projections[20,29]. Corticofugal systems are generally thought to be involved in modulating auditory signal processing. For example, they have been shown to act as a positive feedback to augment the auditory responses of tonotopically matched thalamic or collicular neurons[40–42]. Corticofugal systems are also implicated in mediating activity-dependent plasticity in subcortical structures[40,41,43]. More recently, corticofugal projections to the striatum have been shown to affect decision making during auditory discrimination tasks[25]. Our current results reveal a previously unrecognized functional role of corticofugal projections in mediating innate defense behaviors. In particular, our specific optogenetic manipulations strongly suggest that it is the IC cortex, not the ICC that directly mediates the sound-triggered flight behavior. This finding indicates that ICC and IC cortex are functionally differentiable, and it fits with the anatomical suggestion that the IC cortex may be involved in sensory integration and sensory-motor interaction[29,30,33].

Taken together, the neural pathway from the ACx to the IC cortex and then to the PAG highlights a more active behavioral role of corticofugal projections. By bridging cortical processing of sensory inputs and defensive motor outputs, this pathway may serve not only to amplify innate behavioral responses, but also to provide a route for top-down control of defensive behaviors in general. Since corticofugal projections are prevalent across sensory modalities, it is possible that direct sensory cortical control of defensive behaviors through corticofugal projections is a general strategy exploited by innate defense circuits.

Methods

Head-fixed animal preparation

All experimental procedures used in this study were approved by the Animal Care and Use Committee at the University of Southern California. Male and female C57BL/6J mice aged 6–12 weeks were used in this study. Mice were housed with reversed light-dark cycles with light on from 9:00 PM to 9:00 AM. Flying saucer pet exercise wheels were placed in their home cages. One week before the behavioral tests, animals were prepared in a similar way as previously described[17–19]. The mouse was anesthetized with isoflurane (1.5% by volume) and a screw for head fixation was mounted on top of the skull with dental cement. A ring-like adaptor was glued into the ear that would be contralateral to the sound source for the later ear plugging in some experiments as to avoid the complication of bilateral hearing. Afterwards 0.1mg/kg buprenorphine were injected subcutaneously into the mice before they were returned to home cages.

During the recovery period, the mice were trained to be accustomed to the head fixation on the recording setup. To fix the head, the head screw was tightly fit into a metal post. The animals were allowed to run freely on a flat plate rotating smoothly around its center. One day before electrophysiological recordings or behavioral tests that did not require implantation of cannula, the mouse was anesthetized with isoflurane and a craniotomy was made over the ACx, IC, or SC region accordingly.

The following recordings and tests were all performed in a sound-attenuation booth (Acoustic Systems). The ear contralateral to the sound source was plugged for experiments except those where optogenetic activation was performed. Plugging the ear did not reduce sound triggered running speed compared to conditions when both ears were left open (see Supplementary Fig. 1a). Individual recording sessions lasted for no more than 2 hours. The animal was given drops of 5% sucrose through a pipette every hour. During the test, behaviors of the animal were recorded with a video camera. The rotating speed of the plate was detected with an optical sensor and recorded in real time. The speed of the animal was analyzed both online and offline. Some animals were tested for more than one session, and the two consecutive sessions were separated by at least 1 day.

Behavioral test in freely moving animals

A box with two chambers was used to test the sound triggered flight behavior in freely moving mice. There was one opening connecting the two chambers, allowing the animal to move between the chambers. Animals were allowed to acclimate to the box environment several hours before the behavior test. A speaker was attached to each chamber. Noise was delivered randomly by one of the speakers. Silent sound was delivered with zero sound output. Noise levels in both chambers were measured with a ¼-inch free-field microphone connected with type 2669-L preamplifier (Brüel & Kjær 4939-L-002). There was about 10dB difference between the sound source and the far end of the second chamber. Two cameras were attached to the top of the chambers to monitor the location of the animal. Moving speed was calculated from video images.

In vivo recordings in awake animals

Loose-patch, multiunit and LFC recordings were performed as previously described[18,19], with a patch pipette filled with an artificial cerebral spinal fluid (ACSF; 126 mM NaCl, 2.5 mM KCl, 1.25 mM Na_2PO4, 26 mM $NaHCO_3$, 1 mM $MgCl_2$, 2 mM $CaCl_2$, and 10 mM glucose). Signals were recorded with an Axopatch 200B amplifier (Molecular Devices) under voltage-clamp mode, with a command voltage applied to adjust the baseline current to near zero. Loose-patch recording signals were filtered with a 100–5,000 Hz band-pass filter. LFC signals were low-pass filtered at 300 Hz. The recording sites were marked. The depths of the recorded neurons were determined based on the micromanipulator reading. Recording was performed in a similar way as the whole-cell recording, except that a loose seal (0.1–0.5 giga Ohm) was made on the cell body, allowing spikes only from the patched cell to be recorded. With large pipette openings (impedance < 6 MΩ), no cortical fast-spiking neurons were ever recorded, suggesting that these recording parameters imposed a strong sampling bias towards pyramidal neurons, which have larger cell bodies and more extensive dendritic fields than inhibitory neurons. This bias was also shown in our previous studies[21,44–48].

Recording in the ACx: auditory cortical region was pre-mapped with extracellular recordings, and the primary auditory cortex was identified by its tonotopic representation of characteristic frequencies (CFs) in a caudal-to-rostral (low to high frequency) gradient, relatively sharp spike tonal receptive fields (TRFs) and short onset latencies, as we previously described[19,21]. Recordings from L5 neurons were mostly based on the travel distance of the pipette beneath the pial surface, and verified by histology in some experiments with fluorescence dextran marking, as we described previously[19,21,44,45]. In addition, it is known that ChR2 in the Rpb4-Cre line would be expressed specifically in L5 neurons. Recordings from neurons (presumably excitatory) at the expected depths confirmed that they could respond to LED light illumination (e.g. Fig. 2n).

Recording in the MGBv: We first mapped the auditory thalamus by recording multiunit spikes with a parylene-coated tungsten electrode (2 MΩ, FHC). Mapping was performed in a three-dimensional manner by systematically varying the depth and the x-y coordinates of the electrode which penetrated the primary auditory cortical surface with an approximately right angle. We distinguished the MGBv from other auditory thalamic divisions based on its tonotopic frequency representation, relatively sharp spike TRFs and short onset latencies[21]. Afterwards, cell-attached recordings were made around the central region of the MGBv (approximately 2.4~2.6 mm below the auditory cortical surface).

Recording in the IC: The IC area was first mapped by recording multiunit spikes with a tungsten electrode. The ICC region was identified based on short response latencies (6–10 ms for noise responses), sharply tuned tonal receptive fields as well as a dorsal-to-ventral gradient of characteristic frequencies (from low to high), as described in our previous study[18].

Recording in other midbrain structures: The recordings from PAGd and SC were carried out with glass micro-electrodes. The recording pipette was filled with 0.1 mM fluorescence dextran. After recording, the dye was pressure-injected to the recording area, and the brain was fixed and sectioned to verify the location of the recording.

Viral injection

Viral injections were carried out as we previously described[21]. Adult Rbp4-Cre (MMRRC), Pvalb-Cre × Ai14 tdTomato reporter (The Jackson Laboratory) and wild type C57BL/6J (The Jackson Laboratory) mice were anesthetized with 1.5% isoflurane. A small cut was made on the skin covering the left ACx or IC, and the muscles were removed. Two ~0.2 mm craniotomies were made in the ACx or IC region. The following adeno-associated viruses (AAVs) encoding ChR2, ArchT or GFP were used depending on the purpose of experiments and strain of mice: AAV1.CaMKIIa.hChR2(H134R)-eYFP.WPRE.hGH (UPenn vector core, Addgene 26969), AAV9.EF1α.DIO.hChR2(H134R)-EYFP.WPRE.hGH (UPenn vector core, Addgene 20298), AAV1-CAG-ArchT-GFP (UNC vector core, Addgene 29777), AAV1-CAG-FLEX-ArchT-GFP (UNC vector core, Addgene 28307) and AAV1.CamKII0.4.eGFP.WPRE.rBG (UPenn vector core). The viruses were delivered using a beveled glass micropipette (tip diameter: ~40 μm) attached to a microsyringe pump (World Precision Instruments). For each injection, 100 nl of virus was injected at a rate of 20 nl/min. Right after each injection, the pipette was allowed to rest for 4 minutes before withdrawal. The scalp was then sutured. Following the surgery, 0.1mg/kg buprenorphine was injected subcutaneously before returning the animals back to their home cages. Mice were allowed to recover for at least 3 weeks.

Retrograde Tracer Injection and Imaging

For retrograde tracer injections into IC and SC, 80 nl of fluorescently conjugated Cholera toxin (CTb 555 or 647, 0.25%; Invitrogen) was injected into each location through a pulled glass micropipette using the pressure injection method[49]. Following 5–7 days, animals were deeply anesthetized and transcardially perfused with 4% paraformaldehyde. Brain tissue was sliced into 150 μm sections using a vibratome and sections were mounted onto glass slides and imaged using a confocal microscope.

Sound and LED stimulation

Sound stimulation, LED stimulation and data acquisition software was custom-developed in LabVIEW (National Instruments). For behavioral tests with varying intensities, broadband white noise (1kHz – 64kHz) at nine intensities (10–90 dB SPL spaced at 10 dB) was calibrated and delivered pseudo-randomly through a danish speaker (Scan-speaker D2905). In all other cases, the noise intensity was fixed at 80 dB SPL. The duration of noise was 5 s and the inter-stimulus interval (ISI) was 30 s. The stimulus was repeated 50–80 times to generate an averaged time-dependent speed profile. Note that in quiet conditions animals usually spent only a small fraction of time running, resulting in a low baseline speed. To activate ChR2, a 5-s long train of 10Hz blue LED light pulses (duration of each pulse was 50 ms) was delivered. The intensity of LED was 12 mW (measured at the tip of the fiber). To activate ArchT, a 5-s long train of 10Hz green LED light pulses (duration of each pulse was 50 ms, 12mW) was delivered. The sequence of sound stimulation alone and sound-plus-light combination was randomized.

Optogenetic preparation

To activate or silence IC cortex, an optic fiber (400 μm, Thorlabs) connecting to a blue or green LED source (470 nm and 530 nm, respectively, Thorlabs) was positioned close to the surface of IC cortex. The tip of the optic fiber was covered by agar stained with black pigments to prevent light leakage. Similarly, to activate the ACx or to silence it by activating PV neurons, an optic fiber connecting a blue LED source was placed on the surface of the ACx. The LED-induced behavioral responses could not be attributed to the potential activation of the visual system, since the same optic fiber, when placed on the uninfected ACx, failed to induce changes in running speed (Supplementary Fig. 2e–f). To stimulate deeper structures such as ICC, SC and PAGd, optic fiber patch cord (200 or 400 μm Core, 0.22 or 0.39 NA respectively; Thorlabs) connecting the LED light source to the implanted cannula was secured by a hard plastic sleeve (Thorlabs). The implantation was made in the mouse anesthetized with isoflurane (1.5%) and mounted to the head-fix apparatus. A craniotomy over the target area (ICC, PAGd or ILSC/DLSC) was made. The cannula was lowered with a motion controller (Siskiyou) to the desired depth (ICC: 700 μm; PAGd: 1200 μm; ILSC/DLSC: 800 μm) according to the coordinates in mouse brain atlas. The cannula was then secured on the skull by dental acrylic. All implants were made in left hemisphere. The animals were allowed to rest for at least 2 days before behavioral test sessions. After each experiment, the brain was sectioned and imaged with a fluorescence microscope to confirm the expression of ChR2-EYFP or ArchT-GFP, as well as the location of implanted cannula. To ensure the specificity of optogenetic stimulation, no ChR2 expressing fibers and structures other than the targeted structure should be present in the light pathway from the end of the optic fiber. The axis of the light pathway was the same as the central axis of the optic fiber, and the illumination angle was determined by the fiber's NA value. This rule applied for all of our experiments, and fluorescence expression in the brain sections was examined after each experiment to confirm it.

Silencing of brain structures

We used two methods to silence neural activity. In the first method, fluorescent muscimol or muscimol (1.5 mM, Life Technologies), an agonist of $GABA_A$ receptors, was used to silence a targeted brain region[50]. The muscimol solution (dissolved in ACSF containing fast green) was injected via a glass micropipette with a tip opening of about 2 μm in diameter. To silence the ACx, the pipette was inserted to a depth of 400 μm below the cortical surface. For IC silencing, the pipette was inserted to a depth of 600 μm below the surface. Solutions were injected under a pressure of 2–3 psi for 5 min. The injected volume was estimated to be around 100–150 nl, as measured in mineral oil. The spread of muscimol[51] could be precisely measured by fluorescent imaging. Two hours after injection, the animals were transcardially perfused with 4% paraformaldehyde in phosphate-buffered saline (PFA). 100-μm coronal brain sections were made with a vibratome (Leica Microsystems) and imaged on a confocal microscope (Olympus). The lateral spread of fluorescent muscimol was about 1mm.

For optogenetic silencing, AAV9.EF1α.DIO.hChR2(H134R)-EYFP.WPRE.hGH was injected into the ACx of Pvalb-Cre; Ai14 mice[21,22], or AAV1-CAG-FLEX-ArchT-GFP was injected into the ACx of Rpb4-Cre mice. All the injections targeted the primary auditory

cortical region, but the viral infection was often observed also in the regions surrounding the primary auditory cortex. In each animal, injections were made in 2 sites at 2 depths (300, 600 μm below the surface). After a recovery period of 4–8 weeks, blue LED light was applied to the cortical surface to activate PV neurons, which in turn silenced cortical excitatory neurons[21,22]. As we previously described[21,22], the expression of hChR2(H134R)-EYFP in each injected mouse was examined with a fluorescence microscope before and after the experiments. We found that in all the animals, ChR2 was specifically expressed in PV neurons, and the efficiency of AAV transduction was high (> 80%, see Supplementary Fig. 8), consistent with previous reports[21,22].

Slice preparation and recording

Acute brain slices were prepared from viral injected mice after behavior tests. Following the urethane anesthesia, the animal was decapitated and the brain was rapidly removed and immersed in an ice-cold dissection buffer (composition: 60 mM NaCl, 3mM KCl, 1.25 mM NaH$_2$PO4, 25 mM NaHCO$_3$, 115 mM sucrose, 10 mM glucose, 7 mM MgCl$_2$, 0.5 mM CaCl$_2$; saturated with 95% O$_2$ and 5% CO$_2$; pH= 7.4). Brain slices of 350 μm thickness containing the IC or SC/PAG regions were cut in a coronal plane using a vibrating microtome (Leica VT1000s). Slices were allowed to recover for 30 min in a submersion chamber filled with the warmed (35 °C) ACSF and then to cool gradually to the room temperature until recording. The spatial expression pattern of ChR2-EYFP or ArchT-GFP in each slice was examined under a fluorescence microscope before recording. Only slices with the correct location for expression were used for further recording. Cells were visualized with IR-DIC and fluorescence microscopy (Olympus BX51 WI) for specific targeting of infected neurons. Patch pipettes (Kimax) with ~4–5 MΩ impedance were used for whole-cell recordings. Recording pipettes contained: 130 mM K-gluconate, 4 mM KCl, 2 mM NaCl, 10 mM HEPES, 0.2 mM EGTA, 4 mM ATP, 0.3 mM GTP, and 14 mM phosphocreatine (pH, 7.25; 290mOsm). Signals were recorded with an Axopatch 200B amplifier (Molecular Devices) under voltage clamp mode at a holding voltage of –70mV, filtered at 2 kHz and sampled at 10 kHz. 1 μM TTX and 1 mM 4-aminopyridine (4-AP) was added to the external solution in order to record only monosynaptic responses[15,31].

Photostimulation in slice recording

A mercury Arc lamp was used as the light source. The light was collimated and coupled to the microscope's epifluorescence pathway, and was passed through blue or green filters. A calibrated aperture placed at the conjugated focal plane of the imaged slice was used to control the size of the illumination area. A train of 10Hz blue light pulses (duration of each pulse was 50 ms) was delivered to test the activation of ChR2-expressing neurons. Similarly, a long pulse of green light (duration = 1s) was applied to test the inhibition of ArchT-expressing neurons.

Data analysis

We performed data analysis with custom-developed software (MATLAB, MathWorks). The data were first pooled together for a randomized batch processing and then were categorized according to experimental conditions. The average time-dependent speed profile was

smoothed with a smooth function (rloess) in MATLAB. The speed-intensity curve was fitted with a hyperbolic ratio function:

$$V = V_{\max} \times \frac{I^n}{I^n + I_{50}{}^n} + V_0$$

$V_{\max}$ is the maximum speed, and V_0 is the baseline speed.

Statistics

Shapiro-Wilk test was first applied to examine whether samples had a normal distribution. In the case of a normal distribution, t-test or ANOVA test was applied. Otherwise, a non-parametric test (Wilcoxon signed-rank test in this study) was applied. Data were presented as mean ± s.d.. if not otherwise specified.

Supplementary Material

Refer to Web version on PubMed Central for supplementary material.

Acknowledgments

References

1. Motta SC, et al. Dissecting the brain's fear system reveals the hypothalamus is critical for responding in subordinate conspecific intruders. Proceedings of the National Academy of Sciences of the United States of America. 2009; 106:4870–4875.10.1073/pnas.0900939106 [PubMed: 19273843]

2. Pagani JH, Rosen JB. The medial hypothalamic defensive circuit and 2,5-dihydro-2,4,5-trimethylthiazoline (TMT) induced fear: comparison of electrolytic and neurotoxic lesions. Brain research. 2009; 1286:133–146.10.1016/j.brainres.2009.06.062 [PubMed: 19559688]

3. Blanchard DC, Blanchard RJ. Innate and conditioned reactions to threat in rats with amygdaloid lesions. Journal of comparative and physiological psychology. 1972; 81:281–290. [PubMed: 5084445]

4. Yilmaz M, Meister M. Rapid innate defensive responses of mice to looming visual stimuli. Current biology : CB. 2013; 23:2011–2015.10.1016/j.cub.2013.08.015 [PubMed: 24120636]

5. Litvin Y, Blanchard DC, Blanchard RJ. Rat 22kHz ultrasonic vocalizations as alarm cries. Behavioural brain research. 2007; 182:166–172.10.1016/j.bbr.2006.11.038 [PubMed: 17173984]

6. Choi JS, Brown TH. Central amygdala lesions block ultrasonic vocalization and freezing as conditional but not unconditional responses. The Journal of neuroscience : the official journal of the Society for Neuroscience. 2003; 23:8713–8721. [PubMed: 14507971]

7. Brandao ML, Anseloni VZ, Pandossio JE, De Araujo JE, Castilho VM. Neurochemical mechanisms of the defensive behavior in the dorsal midbrain. Neuroscience and biobehavioral reviews. 1999; 23:863–875. [PubMed: 10541061]

8. Eilam D. Die hard: a blend of freezing and fleeing as a dynamic defense--implications for the control of defensive behavior. Neuroscience and biobehavioral reviews. 2005; 29:1181–1191.10.1016/j.neubiorev.2005.03.027 [PubMed: 16085311]

9. Bandler R, Shipley MT. Columnar organization in the midbrain periaqueductal gray: modules for emotional expression? Trends in neurosciences. 1994; 17:379–389. [PubMed: 7817403]

10. Letzkus JJ, et al. A disinhibitory microcircuit for associative fear learning in the auditory cortex. Nature. 2011; 480:331–335.10.1038/nature10674 [PubMed: 22158104]

11. LeDoux JE. Rethinking the emotional brain. Neuron. 2012; 73:653–676.10.1016/j.neuron. 2012.02.004 [PubMed: 22365542]

12. Johansen JP, Cain CK, Ostroff LE, LeDoux JE. Molecular mechanisms of fear learning and memory. Cell. 2011; 147:509–524.10.1016/j.cell.2011.10.009 [PubMed: 22036561]

13. LeDoux JE. Emotion circuits in the brain. Annual review of neuroscience. 2000; 23:155–184.10.1146/annurev.neuro.23.1.155

14. Maren S. Neurobiology of Pavlovian fear conditioning. Annual review of neuroscience. 2001; 24:897–931.10.1146/annurev.neuro.24.1.897

15. Haubensak W, et al. Genetic dissection of an amygdala microcircuit that gates conditioned fear. Nature. 2010; 468:270–276.10.1038/nature09553 [PubMed: 21068836]

16. Fanselow MS, Poulos AM. The neuroscience of mammalian associative learning. Annual review of psychology. 2005; 56:207–234.10.1146/annurev.psych.56.091103.070213

17. Olsen SR, Bortone DS, Adesnik H, Scanziani M. Gain control by layer six in cortical circuits of vision. Nature. 2012; 483:47–52.10.1038/nature10835 [PubMed: 22367547]

18. Xiong XR, et al. Interaural level difference-dependent gain control and synaptic scaling underlying binaural computation. Neuron. 2013; 79:738–753.10.1016/j.neuron.2013.06.012 [PubMed: 23972599]

19. Zhou M, et al. Scaling down of balanced excitation and inhibition by active behavioral states in auditory cortex. Nat Neurosci. 2014

20. Weiner, JA.; Schreiner, CE. The Inferior Colliculus. Winer, JA.; Schreiner, CE., editors. Springer; 2005. p. 1-68.

21. Li LY, Li YT, Zhou M, Tao HW, Zhang LI. Intracortical multiplication of thalamocortical signals in mouse auditory cortex. Nature neuroscience. 2013; 16:1179–1181.10.1038/nn.3493 [PubMed: 23933752]

22. Li YT, Ibrahim LA, Liu BH, Zhang LI, Tao HW. Linear transformation of thalamocortical input by intracortical excitation. Nature neuroscience. 2013; 16:1324–1330.10.1038/nn.3494 [PubMed: 23933750]

23. Fenno L, Yizhar O, Deisseroth K. The development and application of optogenetics. Annual review of neuroscience. 2011; 34:389–412.10.1146/annurev-neuro-061010-113817

24. Petersen CC, Crochet S. Synaptic computation and sensory processing in neocortical layer 2/3. Neuron. 2013; 78:28–48.10.1016/j.neuron.2013.03.020 [PubMed: 23583106]

25. Znamenskiy P, Zador AM. Corticostriatal neurons in auditory cortex drive decisions during auditory discrimination. Nature. 2013; 497:482–485.10.1038/nature12077 [PubMed: 23636333]

26. Madisen L, et al. A toolbox of Cre-dependent optogenetic transgenic mice for light-induced activation and silencing. Nature neuroscience. 2012; 15:793–802.10.1038/nn.3078 [PubMed: 22446880]

27. Feng G, et al. Imaging neuronal subsets in transgenic mice expressing multiple spectral variants of GFP. Neuron. 2000; 28:41–51. [PubMed: 11086982]

28. Sun YJ, Kim YJ, Ibrahim LA, Tao HW, Zhang LI. Synaptic mechanisms underlying functional dichotomy between intrinsic-bursting and regular-spiking neurons in auditory cortical layer 5. The Journal of neuroscience : the official journal of the Society for Neuroscience. 2013; 33:5326–5339.10.1523/JNEUROSCI.4810-12.2013 [PubMed: 23516297]

29. Huffman RF, Henson OW Jr. The descending auditory pathway and acousticomotor systems: connections with the inferior colliculus. Brain research. Brain research reviews. 1990; 15:295–323. [PubMed: 2289088]

30. Winer JA. Decoding the auditory corticofugal systems. Hearing research. 2006; 212:1–8. [PubMed: 16555378]

31. Petreanu L, Mao T, Sternson SM, Svoboda K. The subcellular organization of neocortical excitatory connections. Nature. 2009; 457:1142–1145.10.1038/nature07709 [PubMed: 19151697]

32. Chow BY, et al. High-performance genetically targetable optical neural silencing by light-driven proton pumps. Nature. 2010; 463:98–102.10.1038/nature08652 [PubMed: 20054397]

33. Gruters KG, Groh JM. Sounds and beyond: multisensory and other non-auditory signals in the inferior colliculus. Frontiers in neural circuits. 2012; 6:96.10.3389/fncir.2012.00096 [PubMed: 23248584]

34. Schenberg LC, et al. Functional specializations within the tectum defense systems of the rat. Neuroscience and biobehavioral reviews. 2005; 29:1279–1298.10.1016/j.neubiorev.2005.05.006 [PubMed: 16087233]

35. Vianna DM, Brandao ML. Anatomical connections of the periaqueductal gray: specific neural substrates for different kinds of fear. Brazilian journal of medical and biological research = Revista brasileira de pesquisas medicas e biologicas/Sociedade Brasileira de Biofisica … [et al.]. 2003; 36:557–566.

36. Winer JA. Decoding the auditory corticofugal systems. Hearing research. 2005; 207:1–9.10.1016/j.heares.2005.06.007 [PubMed: 16091301]

37. Koch M. The neurobiology of startle. Progress in neurobiology. 1999; 59:107–128. [PubMed: 10463792]

38. Koch M, Schnitzler HU. The acoustic startle response in rats--circuits mediating evocation, inhibition and potentiation. Behavioural brain research. 1997; 89:35–49. [PubMed: 9475613]

39. Oliver, DL. The Inferior Colliculus. Winer, JA.; Schreiner, CE., editors. Springer; 2005.

40. Stebbings KA, Lesicko AM, Llano DA. The auditory corticocollicular system: molecular and circuit-level considerations. Hearing research. 2014; 314:51–59.10.1016/j.heares.2014.05.004 [PubMed: 24911237]

41. Suga N, Xiao Z, Ma X, Ji W. Plasticity and corticofugal modulation for hearing in adult animals. Neuron. 2002; 36:9–18. [PubMed: 12367501]

42. Yan W, Suga N. Corticofugal modulation of the midbrain frequency map in the bat auditory system. Nature neuroscience. 1998; 1:54–58.10.1038/255 [PubMed: 10195109]

43. Bajo VM, Nodal FR, Moore DR, King AJ. The descending corticocollicular pathway mediates learning-induced auditory plasticity. Nature neuroscience. 2010; 13:253–260.10.1038/nn.2466 [PubMed: 20037578]

44. Li LY, et al. A feedforward inhibitory circuit mediates lateral refinement of sensory representation in upper layer 2/3 of mouse primary auditory cortex. The Journal of neuroscience : the official journal of the Society for Neuroscience. 2014; 34:13670–13683.10.1523/JNEUROSCI. 1516-14.2014 [PubMed: 25297094]

45. Li LY, et al. Differential Receptive Field Properties of Parvalbumin and Somatostatin Inhibitory Neurons in Mouse Auditory Cortex. Cerebral cortex. 201410.1093/cercor/bht417

46. Sun YJ, et al. Fine-tuning of pre-balanced excitation and inhibition during auditory cortical development. Nature. 2010; 465:927–931.10.1038/nature09079 [PubMed: 20559386]

47. Wu GK, Arbuckle R, Liu BH, Tao HW, Zhang LI. Lateral sharpening of cortical frequency tuning by approximately balanced inhibition. Neuron. 2008; 58:132–143.10.1016/j.neuron.2008.01.035 [PubMed: 18400169]

48. Zhou M, et al. Scaling down of balanced excitation and inhibition by active behavioral states in auditory cortex. Nature neuroscience. 2014; 17:841–850.10.1038/nn.3701 [PubMed: 24747575]

49. Zingg B, et al. Neural networks of the mouse neocortex. Cell. 2014; 156:1096–1111.10.1016/j.cell. 2014.02.023 [PubMed: 24581503]

50. Liu BH, Wu GK, Arbuckle R, Tao HW, Zhang LI. Defining cortical frequency tuning with recurrent excitatory circuitry. Nature neuroscience. 2007; 10:1594–1600.10.1038/nn2012 [PubMed: 17994013]

51. Allen TA, et al. Imaging the spread of reversible brain inactivations using fluorescent muscimol. Journal of neuroscience methods. 2008; 171:30–38.10.1016/j.jneumeth.2008.01.033 [PubMed: 18377997]
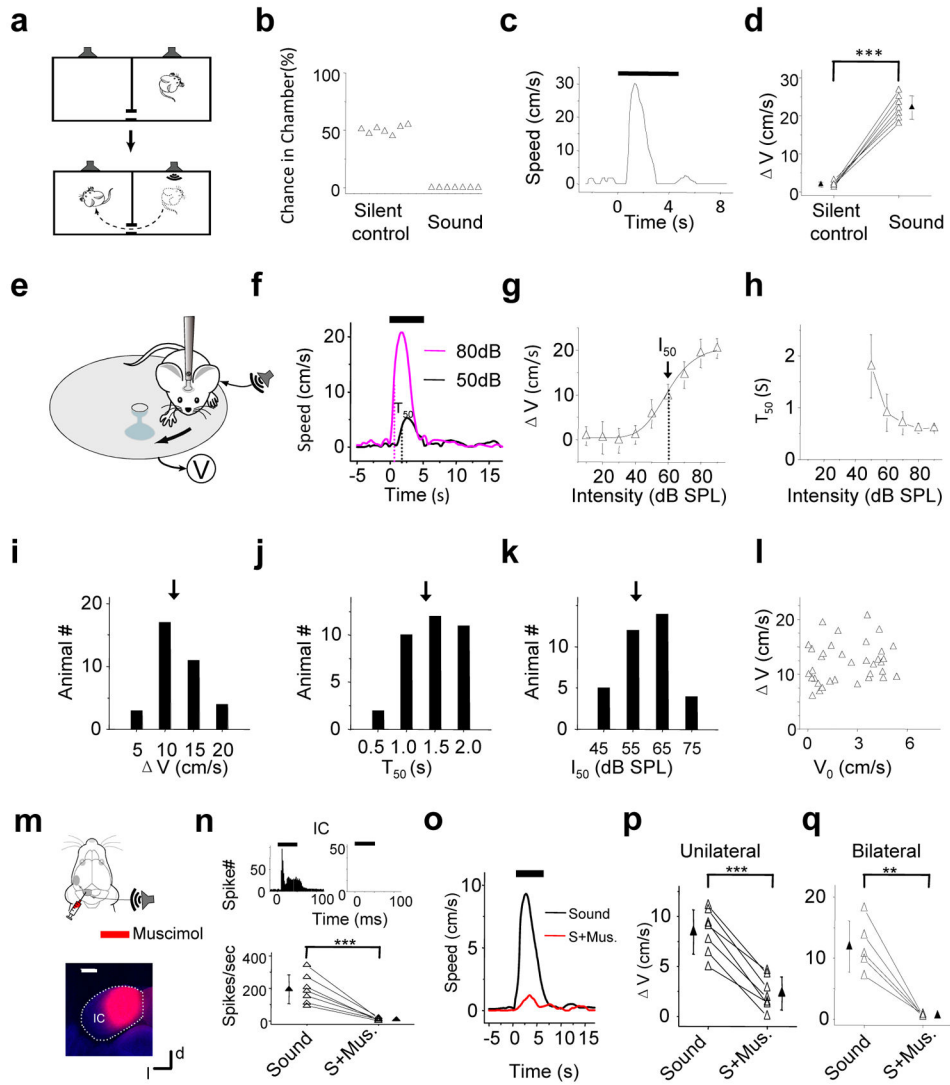
Figure 1. IC-dependent auditory-induced innate flight behavior

(**a**) Schematic graph for the flight behavior test. When sound was played in the chamber the mouse stayed in, it quickly ran to the other chamber. (**b**) Percentage chance of animal staying in the chamber playing sound or silent sound 10 sec after the trigger signal. N = 7 animals. (**c**) Fleeing speed trace for an example animal. Thick bar marks the sound duration. (**d**) Averaged speed of all tested animals (n = 7). ***, P < 0.001, paired t test. (**e**) Head-fixed preparation. Sound was delivered to one ear (with the other ear plugged). Running speed (V) was monitored in real time. (**f**) Average speed of an example animal (50 trials, inter-stimulus interval = 30 s) in response to noise (marked by the thick bar) at two intensity levels. Dash vertical line marks T_{50}. (**g**) Peak induced speed(average of 30 trials or more) versus noise intensity plotted for the same animal in (**f**). Dash vertical line marks I_{50}. (**h**) T_{50} versus noise intensity for the same animal. (**i**) Distribution of average peak induced speeds (n = 35 animals). Arrow marks the mean value. (**j**) Distribution of T_{50} (**k**) Distribution of I_{50}. (**l**) Peak induced versus baseline speed. (**m**) Top, muscimol was injected into the IC contralateral to the sound source. Bottom, fluorescence image of a representative IC slice

showing the spread of muscimol. Scale bar: 500 μm. d, dorsal; l, lateral. (**n**) Top, peri-stimulus spike-time histograms (PSTHs, 100 trials) for responses of an IC neuron to noise before (left) and after (right) muscimol injections. Bottom, average spike rates evoked by noise (80 dB SPL) before and after (S+ Mus.) muscimol injections for 7 IC cells in 7 animals. Recording depths ranged from 250–800 μm. ***, $P < 0.001$, paired t test. (**o**) Speed trace of an example animal before (black) and after (red) muscimol injections into the IC. (**p**) Summary of peak induced speed before and after silencing the contralateral IC. ***, $P < 0.001$, paired t test. N = 7 animals. (**q**) Summary of peak induced speed before and after silencing IC bilaterally. **, $P < 0.01$, paired t test. N = 5 animals. All error bars represent s.d.
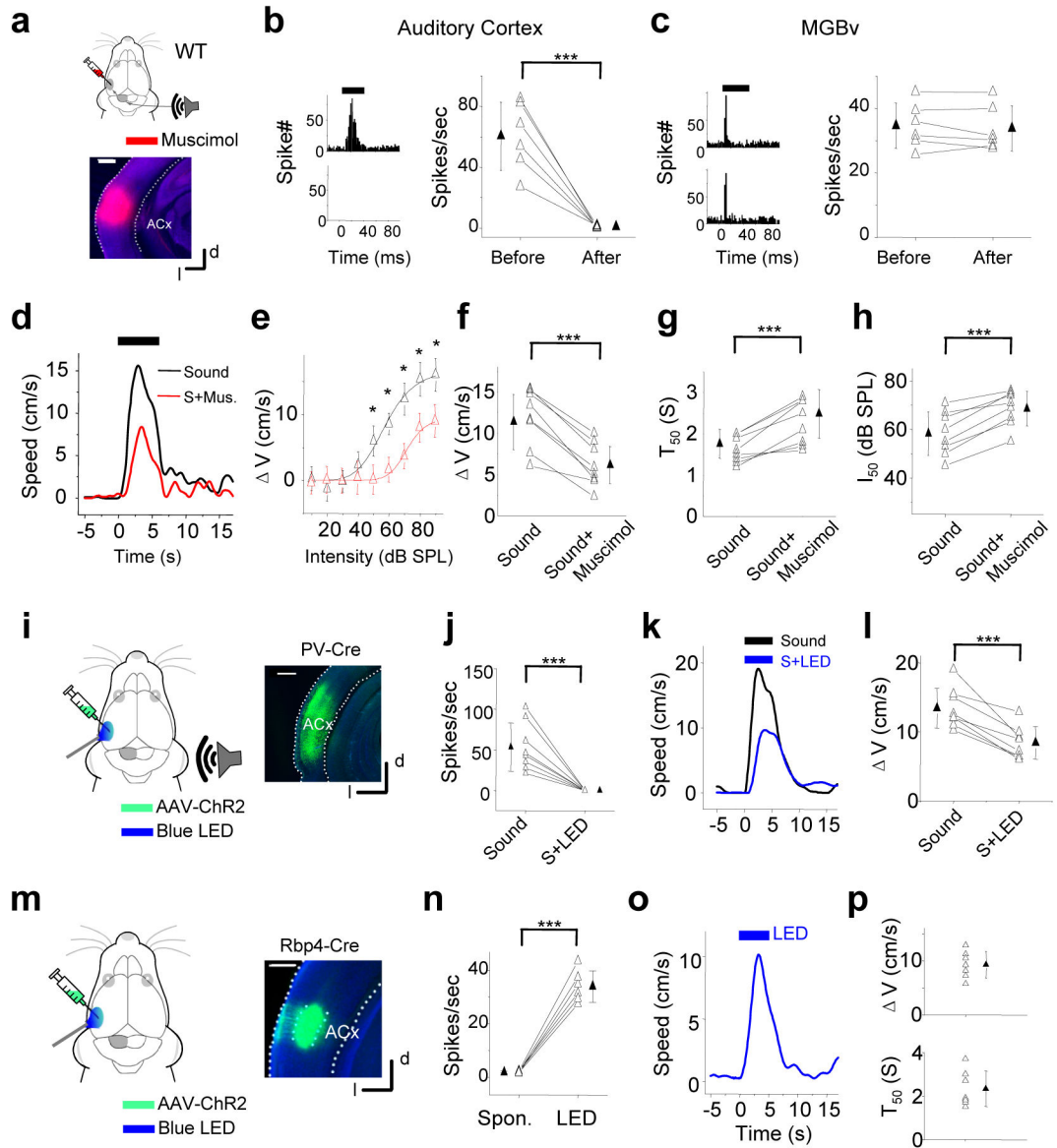
Figure 2. ACx mediates noise-induced flight behaviors

(**a**) Top, experimental condition. Bottom, image showing spread of fluorescent muscimol. (**b**) Left, PSTHs (100 trials) for a cortical L5 neuron's responses to noise (80 dB SPL) before (upper) and after (lower) muscimol injections into the ACx. Right, summary of average spike rates evoked by noise. ***, P < 0.001, paired t test. N = 6 cells in 6 animals. (**c**) Left, PSTHs (100 trials) for an MGBv neuron's responses to noise before (upper) and after (lower) muscimol injections into the ACx. Right, summary of average evoked spike rates for 6 MGBv cells. ***, P < 0.001, paired t test. (**d**) Speed trace for an example animal before (black) and after (red) muscimol injections into the ACx. (**e**) Peak induced speed versus noise intensity for the same animal. *, P < 0.05, two-sample t test. (**f**) Summary of peak induced speed before and after silencing the ACx with muscimol. ***, P < 0.001, paired t test. N = 8 animals. (**g**) Summary of T_{50} ***, P < 0.001, paired t test. N = 8. (**h**)

Summary of I_{50}. ***, $P < 0.001$, paired t test. N = 8. (**i**) Top, experimental condition. Right, image showing ChR2 expression in the ACx. (**j**) Average spike rates of L5 neurons to noise (60 dB SPL)without and with LED illumination. ***, $P < 0.001$, paired t test. N = 8 cells in 3 animals. (**k**) Speed trace of an example animal in response to noise (black) and noise plus LED (blue). (**l**) Average peak induced speed without and with LED illumination. ***, $P < 0.001$, paired t test. N = 8 animals. (**m**) Top: experimental condition. Right, image showing fluorescence labeled layer 5 neurons primarily in the primary auditory cortex (A1). (**n**) Summary of spontaneous firing rates and average multiunit spike rates evoked by LED stimulation (50 ms pulse) in L5 of A1. ***, $P < 0.001$, one sample t test. N = 7 sites in 7 animals. (**o**) Speed trace (average of 35 trials) of an animal in response to LED stimulation. (**p**) Top, summary of peak induced speed to LED stimulation. N = 7 animals. Bottom, summary of T_{50}. All scale bar: 500 μm. All error bars represent s.d.
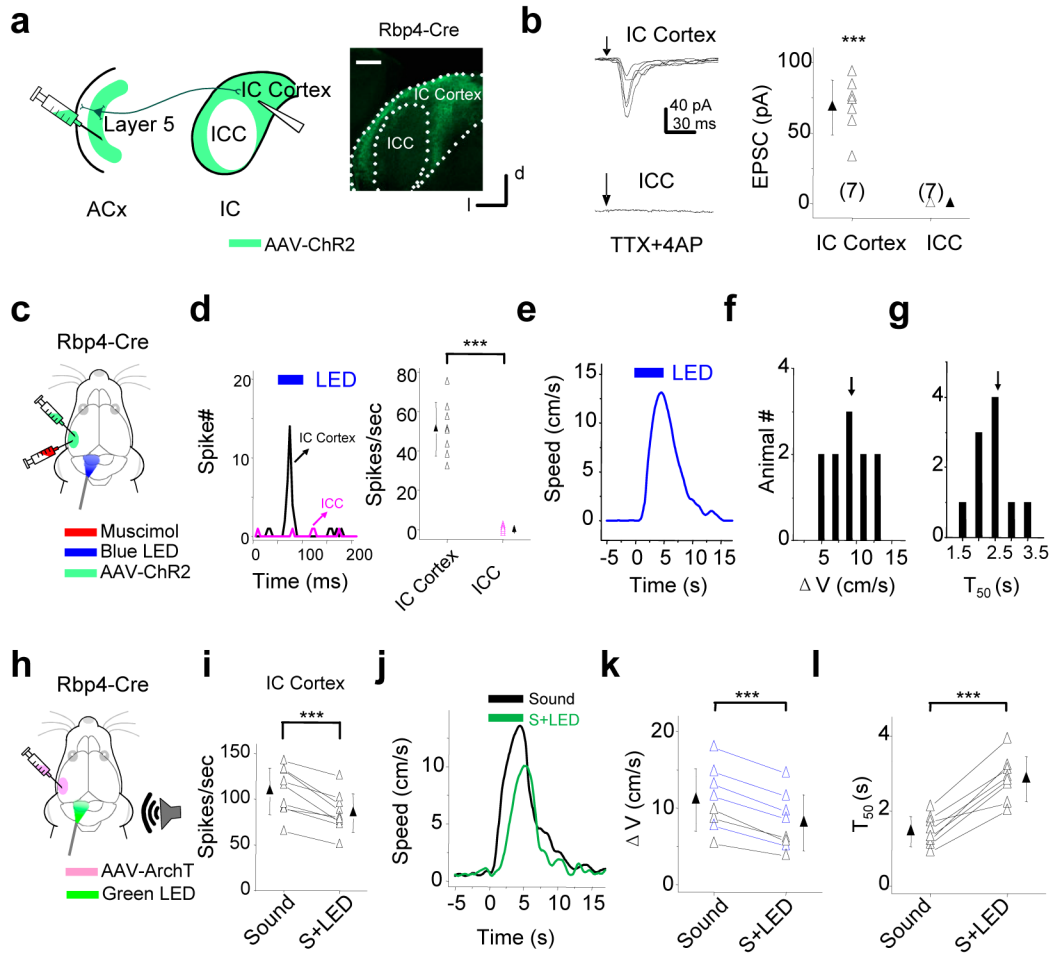
Figure 3. Involvement of corticocollicular projections
(**a**) Left: experimental condition. Right, image showing distribution of corticofugal axons in the IC. Scale bar: 500 μm. (**b**) Left, EPSCs evoked by blue LED illumination (10 ms pulse) in an example IC cortex and ICC neuron, recorded under −70 mV. Arrow marks the onset of LED illumination. Right, summary of average EPSC amplitudes to LED stimulation. ***, different from zero, P < 0.001, t test. N = 7 cells in each group. (**c**) In a head-fixed animal, blue LED light was applied to the IC surface to activate corticocollicular axon terminals with muscimol injected into the ACx on the same side. (**d**) Left, PSTHs (100 trials) of multiunit spike responses to LED illumination (blue bar) in an example IC cortex and ICC recording. Right, summary of average evoked spike rates. ***, P < 0.001, t test. N = 8 sites for each group. (**e**) Speed trace of an example animal in response to the LED illumination on the IC surface. (**f**) Distribution of peak induced speeds to LED stimulation (n = 10 animals). (**g**) Distribution of T_{50}. (**h**) AAV-ArchT was injected into the ACx of a Rbp4-Cre mouse. Weeks later green LED light was applied to the IC on the same side and contralateral to the sound source. (**i**) Average spike rates of IC cortex neurons evoked by noise without and with green LED illumination. ***, P < 0.001, paired t test. N = 9 cells in 5 animals. (**j**) Speed trace of an example animal in response to noise (black) and noise plus green LED illumination (green). (**k**) Summary of peak induced speeds without and with green LED

illumination. ***, $P < 0.001$, paired t test. $N = 8$ animals. Blue symbol labels an individual animal for which there was a significant reduction in speed ($P < 0.05$, t test). (**I**) Summary of T_{50}. ***, $P < 0.001$, paired t test. All error bars represent s.d.
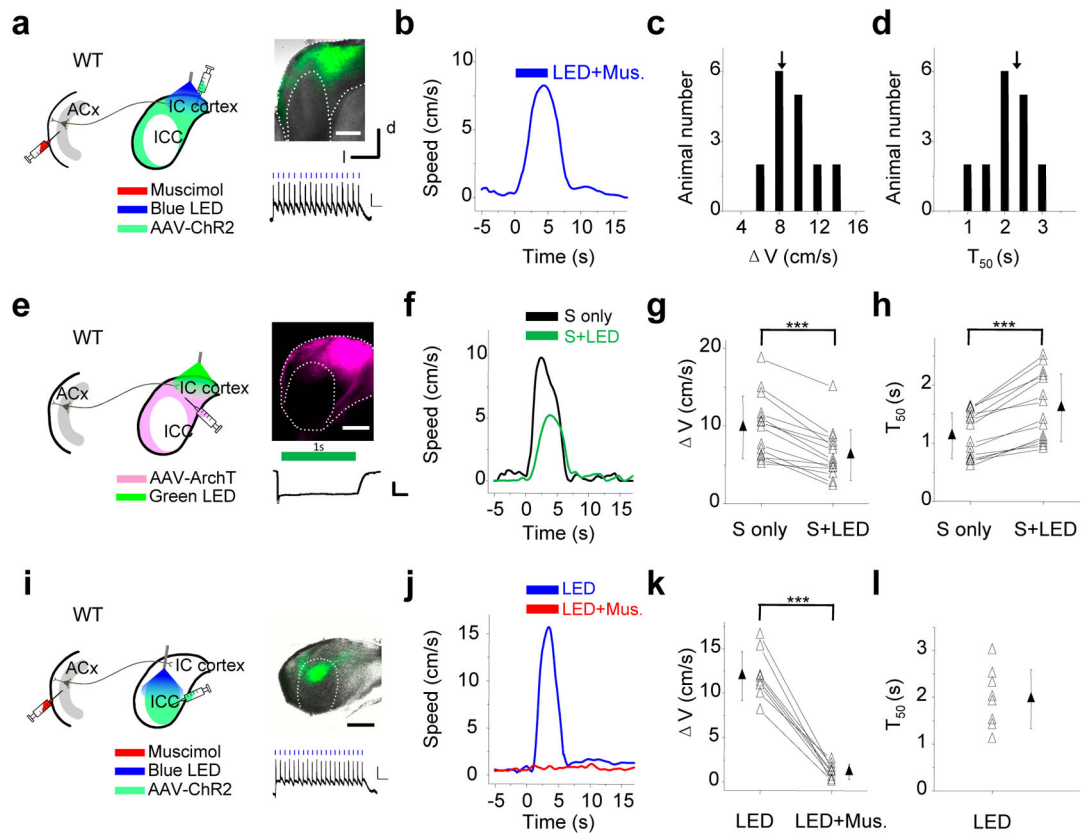
Figure 4. IC cortex mediates the noise-induced fleeing behavior
(**a**) Left, AAV-ChR2-EYFP was injected into the dorsal cortex of IC. Blue LED light was applied to the IC surface while ACx was silenced with muscimol. Right top, fluorescence (green) image superimposed on the bright field image of an IC slice injected with AAV-ChR2. Right bottom, representative membrane potential response of a IC cortex neuron to pulses of LED illumination. Each blue line indicates one pulse. Scale: 25 mV, 200 ms. (**b**) Speed trace of an example animal to blue LED illumination on the IC surface. (**c**) Distribution of average peak induced speeds to LED illumination. N = 17 animals. (**d**) Distribution of T_{50}. (**e**) AAV-ArchT was injected into the dorsal cortex of IC. Green LED light was applied to the IC surface. Right top, fluorescence (pink) image of an IC slice injected with AAV-ArchT. Right bottom, representative membrane potential response of an IC cortex neuron to green LED illumination. Scale: 15 mV, 250 ms. (**f**) Speed trace of an example animal to noise (black) and noise plus green LED illumination (green). (**g**) Summary of noise-induced speed without and with LED illumination. ***, P < 0.001, paired t test. N = 14 test sessions from 7 animals. (**h**) Summary of T_{50}. ***, P < 0.001, Wilcoxon signed rank test. (**i**) AAV-ChR2 was injected into the ICC. Blue LED was applied to the IC surface. The ACx later was silenced with muscimol. Right top, fluorescence (green) image of an IC slice injected with AAV-ChR2. Note that the fluorescence in the IC cortex was attributed to labeled axons from ICC. Right bottom, representative membrane potential response of an ICC neuron to blue LED pulses. Scale: 25 mV, 200 ms. (**j**) Speed trace of an example animal to blue LED illumination before (blue) and after (red) muscimol injections into the ACx. (**k**) Summary of average peak induced speeds to LED illumination before and

after muscimol injections into the ACx. ***, $P < 0.001$, paired t test. N = 10 animals. (**l**) Summary of T_{50}. All scale bar: 500 μm. All error bars represent s.d.
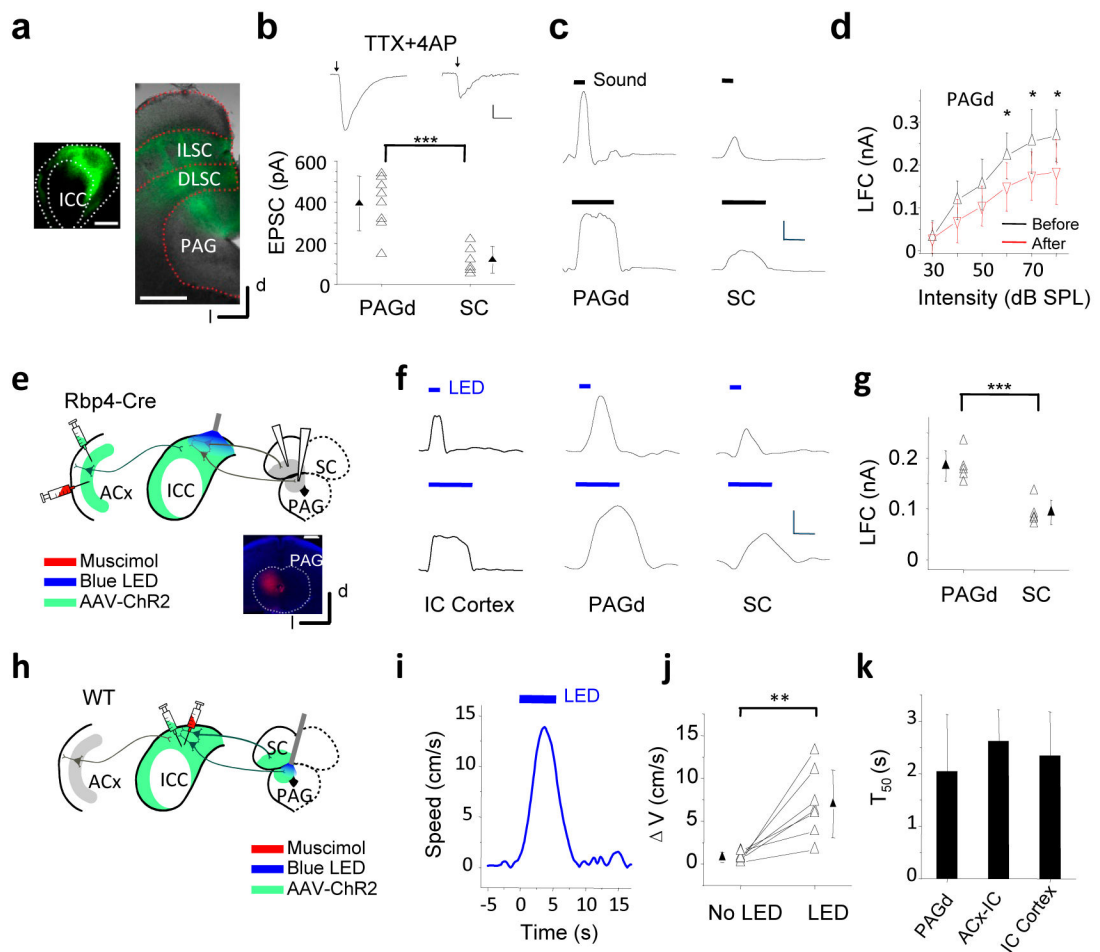
Figure 5. IC cortex drives the midbrain defense system
(**a**) Confocal image of fluorescence labeled axons from the IC cortex in the intermediate layer of SC (ILSC), deep layer of SC (DLSC) and dorsal medial PAG ventral to the SC. Left inset, injection site in the IC cortex. (**b**) Top, average monosynaptic EPSCs recorded in a representative PAGd (left) and SC (right) neuron to LED illumination of ChR2-expressing IC axons. Scale: 50 pA, 30 ms. Bottom, summary of average monosynaptic EPSC amplitudes in PAGd (n = 8) and SC (n = 6) neurons in slice recordings. ***, P < 0.001, two sample t test. (**c**) Local field currents (LFCs) recorded in the PAGd and ventral SC in response to noise of different durations in an example animal. Scale: 0.1 nA, 100 ms. (**d**) Average amplitudes of evoked LFCs at different noise intensities recorded in the PAGd before and after muscimol injections into the ACx. ***, P < 0.001, paired t test. N = 4 animals. (**e**) AAV-ChR2 was injected into the ACx of Rpb4-Cre mice. Blue LED was applied to the IC surface while ACx was silenced with muscimol. Recordings were made in the PAGd and ventral SC. Bottom, image showing injected fluorescent dextran after recording in the PAGd. (**f**) Sample LFCs evoked by LED pulses of different durations recorded in the IC cortex, PAGd and ventral SC, for an example animal. Scale: 0.1 nA, 100 ms. (**g**) Summary of average LFC amplitudes recorded in the PAGd (n = 5 sites from 2 animals) and ventral SC (n = 5 sites from 3 animals). ***, P < 0.001, two sample t test. (**h**)

AAV-ChR2 was injected into the IC cortex. Blue LED was applied to the PAGd, while muscimol was injected into the IC cortex. (**i**) Speed trace of an example animal to blue LED illumination of the PAGd. (**j**) Summary of baseline running speed and average peak induced speed to LED illumination. **, $P < 0.01$, paired t test. N = 7 test sessions from 4 animals. (**k**) Summary of average T_{50} to stimulation of the PAGd, corticofugal axons in the IC and IC cortex neurons. No difference was detected. $P > 0.05$, one-way ANOVA test. All scale bar: 500 μm. All error bars represent s.d.
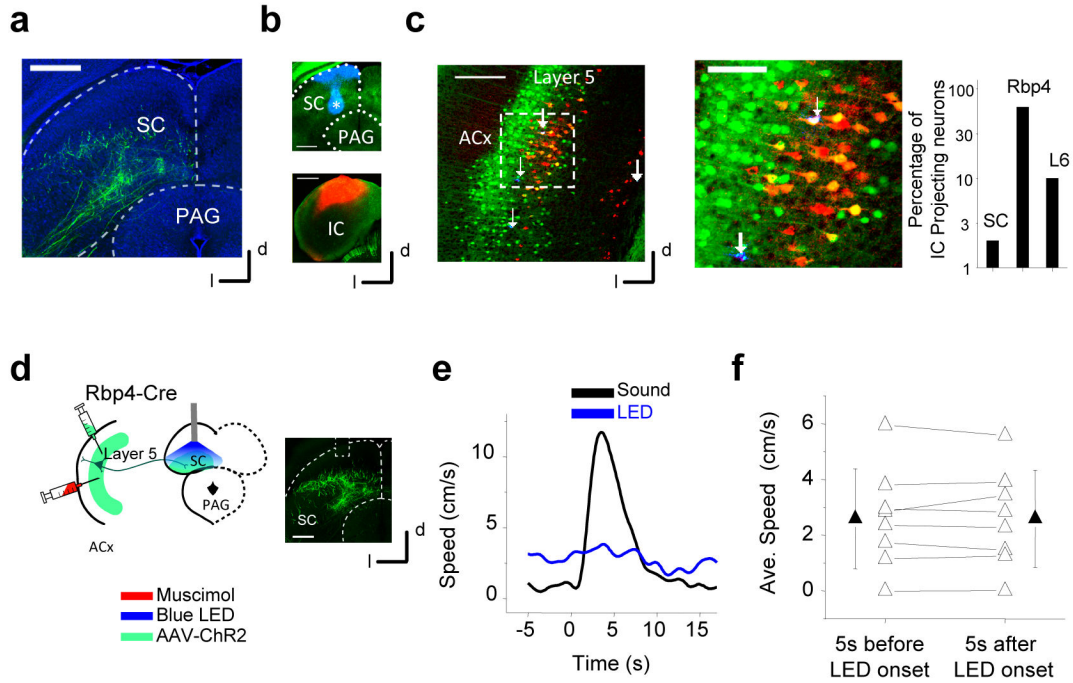
Figure 6. Corticofugal projections to SC unlikely contribute to the noise-induced flight behavior
(**a**) Labeling of corticofugal axons from L5 of the ACx to the intermediate and deep layers of SC. Scale: 500 μm. (**b**) Double injection of two different retrograde tracers into deep layers of SC (blue, top) and the IC cortex (red, bottom) of a Rbp4-Cre GFP mouse. Scale: 500 μm. Note that the blue staining in the superficial layer of SC was due to leakage (injection site marked by *). (**c**) Left, retrograde labeling of SC- and IC-projecting neurons in the ACx. Red neurons project to the IC, blue neurons (marked by white arrows) to the SC. SC-projecting neurons are scarce (only 4 neurons in the view field). Scale: 250 μm. Middle, a blow-up image of the boxed area on the left. One out of four SC-projecting neurons also projects to the IC (labeled by white color). Scale: 100 μm. Right, percentage overlap between retrogradely labeled IC projecting cortical neurons with retrogradely labeled SC-projecting cortical neurons, genetically labeled L5 cells in the Rpb4-Cre mouse and with layer 6 neurons. (**d**) Injection of AAV-ChR2-EYFP labeled L5 axon terminals in SC deep layers. Blue LED was applied to the SC, while the ACx was silenced with muscimol. Right, fluorescence image showing the ACx-SC axon terminals and optic fiber placement. Scale: 500 μm. (**e**) Speed trace of an example animal in response to blue LED illumination of the SC (blue), and to 80 dB SPL noise (black). (**f**) Speeds averaged within 5-s window before and after the onset of LED illumination in SC deep layers. N = 8 animals. No difference was detected. P = 0.97, two sided paired t test. All error bars represent s.d.
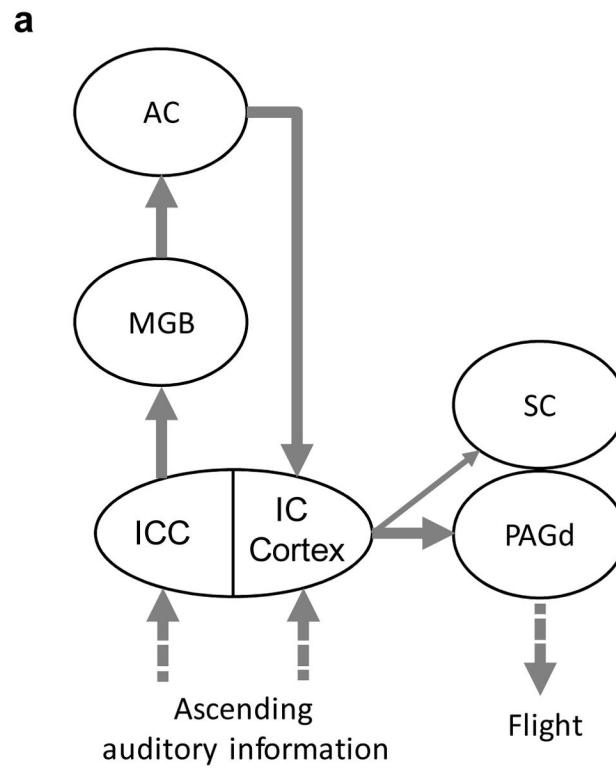
a

Figure 7. Schematic illustration of the neural pathways underlying the sound-evoked flight behavior

Note that besides the feedback projection from the ACx, the IC cortex (ICx) in the midbrain also receives direct ascending auditory inputs from lower brainstem nuclei.